Journal of Nuclear Materials 384 (2009) 12–18

Contents lists available at ScienceDirect

Journal of Nuclear Materials

journal homepage: www.elsevier.com/locate/jnucmat

Model for evolution of crystal defects in UO_2 under irradiation up to high burn-ups

M.S. Veshchunov *, V.E. Shestak

Nuclear Safety Institute (IBRAE), Russian Academy of Sciences, 52, B. Tulskaya, Moscow 115191, Russian Federation

ARTICLE INFO

Article history:
Received 28 May 2008
Accepted 28 September 2008

ABSTRACT

The model for dislocations evolution under irradiation conditions in UO_2 is developed and implemented in the MFPR code. Being combined with the MFPR set of microscopic equations for the evolution of point defects and their interactions with gas bubbles, a self-consistent consideration of the whole system of point and extended defects in irradiated fuel, including point defects (vacancies, interstitials and gas atoms), as well as extended defects (bubbles, dislocations, vacancy loops and pores), is attained. The MFPR code with the new defect evolution model is successfully validated against steady-irradiation experiments, in which the dislocation density and the bubble concentration and mean size were directly measured as functions of burn-up at ≈1000 K. Being applied to higher temperatures, the code allows mechanistic interpretation of the temperature threshold for the fuel restructuring observed in the rim-zone of high burn-up UO_2 fuel.

1. Introduction

One of the main deficiencies of existing fuel performance codes is connected with an oversimplified consideration of microscopic defects in the UO_2 crystal structure, which can strongly influence fission products transport out of grains and release from fuel pellets. Hence, the basic postulation of these codes is based on consideration of equilibrium state of intra-granular gas bubbles formed from the solid solution of gas atoms in the UO_2 matrix under irradiation conditions. Such an approach radically simplifies the theory, since in this case the defect structure of the crystal (including point defects, such as vacancies and interstitials, and extended defects, such as dislocations) is practically excluded from consideration. In particular, this consideration is well grounded only in the initial stage of steady-state irradiation, when the density of generated dislocations is relatively low. At high burn-ups the dislocation density significantly increases [1] and influences the intra-granular bubbles evolution. Namely, considerable suppression of the intra-granular bubble generation leading to a stabilisation of their concentration in the late stage of irradiation accompanied by a noticeable increase in the mean bubble size, was observed in high burn-up UO_2 fuel [2], in remarkable contradiction with standard code's predictions.

Furthermore, under transient and/or annealing conditions the approximation of equilibrium bubbles is no longer valid, and interactions of bubbles with point defects and dislocations become essential. Lacking a mechanistic description of real defects (vacancies, interstitials and dislocations) and their interactions with bubbles, various artificial mechanisms were introduced into the codes, in order to simulate more complicated regimes. These artificial mechanisms require 'effective' parameters, which introduce strong uncertainties in code predictions and, as a result, the advantage of the mechanistic approach is essentially lost. Trying to avoid any artificial tuning and introduction of artificial mechanisms were important reasons for the development of the code MFPR (Module for Fission Products Release) [3,4].

In the present model, dislocations are generated under irradiation in the form of di-interstitials and continuously grow by absorption/evaporation of point defects in two types, dislocation loops and dislocation network, as observed in [5,6] (see below). In order to simplify the system of equations in MFPR, the mean-field approximation for the loop evolution (characterised by the mean radius growth) and transformation into dislocation network, is applied in the current approach.

According to experimental observations, the generation of dislocation loops occurs mainly during the initial period of irradiation, concurrently with the fuel densification process, and therefore, may be significantly influenced by the kinetics of pore sintering. Consequently, in the MFPR code both processes of dislocation loops generation and pore shrinkage are considered simultaneously and self-consistently with point defect and gas bubble evolution.

After implementation of the new model in the MFPR code, additional parameters characterising the crystal defect structure naturally arise. However, being physically grounded, these new microscopic parameters can be fixed from the analysis of available experimental data, and then used without any artificial tuning in further calculations (in contrast to the above-mentioned 'effective'

* Corresponding author. Tel.: +7 495 955 2218; fax: +7 495 958 0040.
E-mail address: vms@ibrae.ac.ru (M.S. Veshchunov).

0022-3115/$ - see front matter © 2008 Elsevier B.V. All rights reserved.
doi:10.1016/j.jnucmat.2008.09.024

parameters). Results of the defect model validation against the tests [1,2] (in which variation of the dislocation density and intra-granular bubbles concentration and size were directly measured with burn-up), are presented.

The new model with the microscopic parameters fitted during validation, is further applied to analyse high burn-up fuel over a wide temperature range; this allows mechanistic interpretation of the temperature threshold for fuel restructuring and rim-zone formation, recently observed in the high burn-up UO_2 fuel [7].

2. Evolution of point defects (vacancies and interstitials)

Evolution of the vacancy and interstitial distribution under irradiation is described in MFPR via the mean field approximation [8] in terms of the dimensionless concentrations, c_v and c_i (the number of vacancies and interstitials per uranium atom), by the following equations:

$$\dot{c}_v = -(k_v^2 + k_{v,g,b}^2)D_v c_v - \alpha D_i c_i c_v + (1-\xi)K + K_e + K_b + K_p, \quad (1)$$

$$\dot{c}_i = -(k_i^2 + k_{i,g,b}^2)D_i c_i - \alpha D_i c_i c_i + K - K_d, \quad (2)$$

where D_v and D_i are the vacancy and interstitial diffusion coefficients, respectively; $\alpha = 4\pi r_c/\Omega$ is the recombination constant; k_v^2 and k_i^2 are the total sink strengths of vacancies and interstitials into extended defects (gas bubbles, pores, vacancy and interstitial loops and dislocations), respectively; $k_{v,g,b}^2$ and $k_{i,g,b}^2$ are the grain boundary sink strengths for vacancies and interstitials, respectively; K is the Frenkel pair production rate (d.p.a. s^{-1}), which can be estimated (for PWR normal operation conditions) by $K = Fz_s\Omega$, where F is the fission rate and the parameter $z_s = (1–5)\cdot 10^5$ characterises the damage formation in the fission track volume [9]; ξK is the rate at which vacancies are removed from solution to form vacancy loops, ξ is the adjustable parameter, $0 < \xi << 1$ [10,11]; K_e is the rate at which thermal vacancies are produced; K_p is the rate of irradiation re-solution (knockout) of vacancies from pores; K_b is the rate of the irradiation induced re-solution of vacancies from gas bubbles; K_d is the rate of the interstitial absorption due to the interstitial loop generation.

The grain boundary sink strength for vacancies and interstitials are evaluated from the relationship [8]:

$$k_{g,b}^2(i,v) = \frac{k_{i,v}R_g\coth(k_{i,v}R_g) - 1}{R_g^2\left[\frac{1}{3} + \frac{1}{k_{i,v}^2R_g^2} - \frac{\coth(k_{i,v}R_g)}{k_{i,v}R_g}\right]}. \quad (3)$$

In accordance with [8,10,11], the total sink strength due to vacancies and interstitials, $k_{v,i}^2$, is determined from:

$$k_{i,v}^2 = 4\pi R_b C_b + 4\pi R_p C_p + Z_{i,v}(\rho_d + 2\pi R_l C_l + 2\pi R_{vl}C_{vl}). \quad (4)$$

The rate of the vacancy thermal production has the form:

$$K_e = D_v\left[4\pi R_b C_b c_v^{(bs)} + 4\pi R_p C_p c_v^{(ps)} + Z_v(\rho_d + 2\pi R_l C_l + 2\pi R_{vl}C_{vl})c_v^{(eq)}\right], \quad (5)$$

where $c_v^{(eq)}$ is the thermal equilibrium vacancy concentration; $c_v^{(bs)}$ and $c_v^{(ps)}$ are the boundary concentrations of vacancies near the bubble and pore surfaces, respectively; ρ_d is the dislocation network density; C_b and R_b are the gas bubbles concentration and mean bubble radius; C_p and R_p are the pore concentration and mean radius, respectively; C_{vl} and R_{vl} are the vacancy clusters (loops) concentration and mean radius; C_l and R_l are the interstitial loops concentration and mean radius.The vacancy production rate from pores due to knockout by fission fragments passing through pores, described in [12], has the form:

$$K_p = 4\pi R_p^2 C_p 2\Omega F\lambda\eta, \quad (6)$$

where the number of vacancies knocked out of a pore per collision, $\eta = 100$, and the length of the fission fragment path, $\lambda = 10^{-6}$ m, in accordance with estimations given in [11].

The vacancy production rate from bubbles due to knockout by fission fragments passing through bubbles, which was introduced in [13] as the thermal annealing of bubbles (to equilibrium volume) in the molten zone of fission tracks, can be represented in the form:

$$K_b = 4\pi R_b C_b\left[D_v\left(c_v - c_v^{(eq)}\right) - D_i c_i\right] - \frac{d(C_b V_b)}{dt}, \quad (7)$$

i.e. as a difference between the rate balance of point defects sinking into bubbles and the real rate of bubble volume growth. In this case, the bubbles are considered as equilibrium (owing to their thermal annealing in fission tracks) and their growth is determined by absorption of gas atoms (as the rate controlling step). In accordance with the 'thermal spike' model [14], molten zones appear in the fission tracks during some time interval $\tau^* \approx 10^{-11}$ s, which is long enough for relaxation of small nanometre bubbles to the equilibrium ('capillary') state in the melt, as explained in [13].The rate of interstitial absorption due to interstitial loop generation in the mean field approximation for loops (see below Eq. (23)) is equal to

$$K_d = \pi R_l^2 b\frac{dC_l}{dt}, \quad (8)$$

where b is the Burgers vector length.

The dislocation sink strength for interstitials is larger than that for vacancies due to the higher elastic interaction between dislocations and interstitials [8]

$$Z_i = Z_v(1+2\varepsilon)0 < 2\varepsilon \ll 1. \quad (9)$$

The thermal equilibrium vacancy concentration, $c_v^{(eq)}$, and interstitial concentration, $c_i^{(eq)}$, are approximated by the Arrhenius correlation:

$$c_{v,i}^{(eq)} = \exp\left(-E_{v,i}^{(eq)}/kT\right), \quad (10)$$

with the activation energies $E_v^{(eq)} = 2.2$ eV and $E_i^{(eq)} \approx 6.0$ eV [15].

The interstitial diffusivity may be given either by the expression:

$$D_i = \frac{2}{3}x_i^2 a^2 \nu_i \exp\left(-E_i^{(m)}/kT\right), \quad (11)$$

where $\upsilon_i = 5\times 10^{12}\ s^{-1}$ is the jump frequency, $E_i^{(m)} = 0.6$ eV is the migration activation energy, $x_i^2 = 10^2 \div 1$ is deviation from stoichiometry factor as justified in [16]; or

$$D_i = \left(\frac{a}{2}\right)^2 \nu_i \exp(-28000/RT), \quad (12)$$

where $\upsilon_i = 10^{13}\ s^{-1}$ is the interstitial jump frequency, $a = 5.5\cdot 10^{-10}$ m is the lattice parameter and $R = 8.314\ J\ mol^{-1}\ K^{-1}$ [17].

The uranium self-diffusion coefficient D_U at low temperatures (below ≈1000 °C), under steady irradiation conditions, is completely athermal and depends only on the fission rate F [17]. At higher temperatures, D_U slowly increases with temperature up to its thermal value (attained at ≈1500 °C). So the uranium self-diffusion coefficient may be evaluated as the sum of two (athermal and thermal) terms:

$$D_U = AF + D_U^{(0)}\exp\left(-\frac{E_U}{kT}\right), \quad (13)$$

with $A \approx 1.2\times 10^{-39}\ m^5$, $D_U^{(0)} = 2\times 10^{-4}\ m^2/s$ and $E_U/k = 64,200$ K [17].

The athermal diffusivity can be reasonably evaluated within the so-called 'thermal rods' mechanism [18], which describes

enhanced migration of U atoms in the molten zones of fission tracks during the short period of the thermal spike. Within this mechanism one should also take into consideration that existing point defects recombine in the molten zones of the fission tracks, thus, in the recrystallised material all interstitials will be annealed (since $c_i \ll c_v$), whereas vacancies will be spatially redistributed (owing to U atoms transport in the melt). Therefore, enhanced migration of U atoms in molten tracks leads to enhancement of the effective vacancy diffusivity (and does not influence the interstitial diffusivity).

Furthermore, the uranium self-diffusion coefficient D_U can be generally represented as superposition of the vacancy and interstitial migration mechanisms:

$$D_U \approx D_v c_v + D_i c_i, \tag{14}$$

which become comparable under steady state low temperature irradiation conditions, as follows from Eqs. (1) and (2) (see, e.g., [13]):

$$D_i c_i \approx D_v c_v (k_v^2/k_i^2) \approx D_v c_v, \tag{15}$$

and, thus,

$$D_U \approx 2 D_v c_v \approx 2 D_i c_i. \tag{16}$$

Therefore, the effective vacancy diffusivity D_v can be calculated from Eqs. (13) and (16) using steady-state solution of Eqs. (1) and (2) for c_v and c_i with D_i defined in Eq. (11) or Eq. (12).

At high temperatures ($T \geqslant 1500$ °C) the thermal effects dominate over irradiation effects and the steady state vacancy concentration is determined by its thermal equilibrium value, $c_v \approx c_v^{(eq)}$, so that

$$D_U \approx D_v c_v \gg D_i c_i, \tag{17}$$

instead of Eq. (16) (see, e.g., [13]).

3. Evolution of extended defects (bubbles, pores and dislocations)

The boundary concentrations of vacancies near the bubble and pore surfaces are given by

$$c_v^{(bs)} = c_v^{(eq)} \exp\left(-\Omega \delta P_b / kT\right), c_v^{(ps)} = c_v^{(eq)} \exp\left(-\Omega \delta P_p / kT\right). \tag{18}$$

The difference between the actual and equilibrium bubble (pore) gas pressures, $\delta P_{b,p}$, is defined as

$$\delta P_j = P_j - P_h - \frac{2\gamma}{R_j}, P_j = \frac{N_j kT}{(V_j - B_{Xe} N_j)}, \quad j = b, p, \tag{19}$$

where P_h is the external hydrostatic pressure, γ is the effective surface tension for UO_2, $P_{b,p}$ is the gas pressure in a bubble or pore, given by the Van-der-Waals equation, $N_{b,p}$ is the number of gas atoms in a bubble or pore, $V_{b,p} = x_{b,p}\Omega$ is the bubble or pore volume, comprising of $x_{b,p}$ U vacancies with the volume $\Omega \approx 4.1 \times 10^{-29}$ m^3, and $B_{Xe} \approx 8.5 \times 10^{-29}$ m^3 is the Van-der-Waals constant for xenon ($B_{Xe} \approx 2\Omega$).

In the case of steady state irradiation conditions, the bubble volume V_b can be calculated using the equilibrium equation, $\delta P_b = 0$, and the corresponding boundary condition, Eq. (18), takes the form $c_v^{(bs)} = c_v^{(eq)}$.

Following [13] it is assumed that the nucleation factor F_n entering transport equations for the intra-granular gas-bubble system and determining the probability that two gas atoms in UO_2 that have come together actually stick and form a bubble, is proportional to the probability that a vacancy is located in a certain position (collision of two atoms), and therefore is equal to the vacancy concentration c_v.

Indeed, this can be demonstrated if one formally extends the Van-der-Waals state equation, Eq. (19), to small bubbles formed by $N = 2$ gas atoms and x vacancies. According to simulations [19,20], gas atoms in UO_2 diffuse in clusters with U (and O) vacancies. In this case, at least one additional U vacancy is necessary to form, after collision of two atoms, a stable bubble obeying a restriction $x > 2N$ of the above-presented Van-der-Waals equation, represented in the form: $NkT = P_b(x\Omega - B_{Xe}N) \approx P_b\Omega(x - 2N)$. This important conclusion, based on the formal extension of the Van-der-Waals state equation to the bubble nucleus, can be apparently confirmed with atomistic computer calculations.

The probability that a vacancy is located in a certain position (of a two atoms collision) is equal to the vacancy bulk concentration c_v. Therefore, the nucleation factor is calculated in a self-consistence manner as

$$F_n = c_v. \tag{20}$$

Following [11], the main equation for the evolution of pores has the form:

$$\frac{dV_p}{dt} = 4\pi R_p (D_v(c_v - c_v^{(ps)}) - D_i c_i) - 4\pi R_p^2 2\Omega F \lambda \eta, \tag{21}$$

with parameters λ and η defined in Eq. (6).

The vacancy cluster (loop) concentration is found from the equation [10,11]:

$$\frac{d}{dt} C_{vl} = -\frac{2\pi R_{vl}}{\Omega_{vl}} \left[Z_i D_i c_i - Z_v D_v (c_v - c_v^{(eq)})\right] C_{vl} + \frac{\xi K}{\Omega_{vl}}, \tag{22}$$

where the vacancy cluster mean volume is $\Omega_{vl} \equiv \pi R_{vl}^2 B$.

The nucleation rate of (interstitial type) dislocation loops is determined by formation (and following growth) of di-interstitial clusters (see, for example, [21]). Therefore, in the mean field approximation the dislocation loop concentration is calculated as

$$\frac{dC_l}{dt} = \frac{\alpha_l D_i c_i^2}{\Omega}, \tag{23}$$

where α_l is the dislocation loop nucleation constant, $D_i\alpha_l = 4\pi r_{ii}(D_i + D_i)/\Omega = 8\pi r_{ii} D_i/\Omega$. Under an assumption $r_{ii} \approx r_{iv} \equiv r_c$, one can estimate $\alpha_l \approx 2\alpha$, where $\alpha = 4\pi r_{iv}(D_i + D_v)/\ \Omega D_i \approx 4\pi r_{iv}/\Omega$ is the vacancy–interstitial recombination constant (see Eqs. (1) and (2)). Ionic charge effects (discussed, for example, in [16]) can violate the assumption $r_{ii} \approx r_{iv}$ and therefore, change the values of the constants α_l and α. It is usually assumed [22] that dislocation loops are generated during the initial stage of irradiation until:

$$D_i c_i - D_v (c_v - c_v^{(eq)}) > 0. \tag{24}$$

This stipulation can be simply justified if one notices that a dislocation bias for interstitials (due to elastic interactions of dislocations with point defects) takes place for finite loops, but not for small di-interstitial clusters. This implies that when, after some initial period of irradiation, $D_i c_i - D_v (c_v - c_v^{(eq)})$ becomes non-positive, the small clusters will not be stable and thus will disappear, whereas loops already formed may proceed to grow owing to a non-zero bias factor ε, in accordance with results presented below, i.e. Eq. (25).

This conclusion is also in fair agreement with direct observations [5,6]. In these tests the UO_2 specimens were irradiated in a neutron flux of 1.4×10^{18} slow neutrons $\cdot$m^{-2}, which induced a fission rate of 1.2×10^{20} m^{-3} s^{-1} in the specimens. At low doses, dislocation loops, formed from platelets of interstitial atoms, were produced. These became resolvable in the electron microscope as 2.5 nm diameter black spots at a dose of 4×10^{21} m^{-3}, and grew in area proportional to the total dose. After a dose of 10^{24} m^{-3}, these dislocation loops had grown sufficiently to coalesce with neighbouring loops to form a dislocation network. With further

increase in dose to $2.2 \times 10^{25}\ \mathrm{m}^{-3}$, the network coarsened with a dislocation density of $2 \times 10^{13}\ \mathrm{m}^{-2}$.

The mean dislocation loop radius growth rate obeys the following equations [22]:

$$\begin{cases} \frac{dR_l}{dt} = \frac{2\pi}{b\ln\left(8R_lR_d^{-1}\right)}\left[(1+2\varepsilon)D_ic_i - D_v(c_v - c_v^*)\right], & \text{if } R_l < R_s = \left(\frac{3}{4\pi C_l}\right)^{\frac{1}{3}}, \\ \frac{dR_l}{dt} = \frac{2\pi}{b\ln\left(\pi\rho_dR_d^2\right)^{-1/2}}\left[(1+2\varepsilon)D_ic_i - D_v(c_v - c_v^*)\right], & \text{if } R_l \geq R_s. \end{cases} \tag{25}$$

where R_s characterises the mean distance between dislocations, R_d is the dislocation core radius estimated as $R_d \cong 3b$, b is the Burgers vector length, $c_v^* = c_v^{(eq)}\exp(-(\gamma_f + E_l)\Omega/bkT)$ is the boundary vacancy concentration at a dislocation loop, γ_f denotes the stacking fault energy, Ω is the atomic volume, E_l is the dislocation loop elastic energy, which is determined from

$$\begin{cases} E_l = \frac{E_{UO_2}b}{2(1-\nu_{UO_2}^2)4\pi}\frac{1}{\left(1+\frac{R_l}{b}\right)}\ln\left(1+\frac{R_l}{b}\right), & \text{if } R_l < R_s = \left(\frac{3}{4\pi C_l}\right)^{\frac{1}{3}}, \\ E_l = 0, \ \text{if } R_l \geq R_s, \end{cases} \tag{26}$$

where at $R_l \geq R_s$ the dislocation loops are approximated as straight dislocations (see Eq. (28) below), e.g. $R_l \to \infty$.

The Poisson's ratio and Young's modulus of UO_2 in Eq. (26) can be determined using the data from [23]:

$$E_{UO_2} = 2.334 \cdot 10^{11}(1 - 1.0915 \cdot 10^{-4}T)\exp(-\beta x),$$
$$\nu_{UO_2} = 0.316,$$

where T is the fuel temperature; x is the magnitude of deviation from stoichiometry in $UO_{2\pm x}$ fuel; β is 1.34 for hyperstoichiometric fuel or 1.75 for hypostoichiometric fuel [23].

However, in experimental observations [1,5] only perfect dislocations with Burgers vector $\vec{b} = \frac{1}{2}[1\,1\,0]$ (i.e. without dissociation into partial dislocations and formation of stacking faults, typical for the fcc-lattice metals) were evidenced. For this reason, only perfect dislocations without stacking faults will be considered in further calculations:

$$c_v^* = c_v^{(eq)}\exp\left(-\frac{E_l\Omega}{BkT}\right). \tag{27}$$

The dislocation sink strength for vacancies is evaluated in [22] as

$$Z_v = \begin{cases} 2\pi\left[\frac{1}{\ln(\pi\rho_dR_d^2)^{-1/2}} + \frac{2\pi R_lC_l}{\rho_d\ln(8R_lR_d^{-1})}\right], & \rho_d(t) = \rho_d(0), \\ \quad \text{if } R_l < R_s = \left(\frac{3}{4\pi C_l}\right)^{\frac{1}{3}}; \\ 2\pi\frac{1}{\ln(\pi\rho_dR_d^2)^{-1/2}}, \quad \rho_d(t) = \rho_d(0) + 2\pi R_lC_l, & \text{if } R_l \geq R_s, \end{cases} \tag{28}$$

where $\rho_d(0)$ is the initial network dislocation density. In this approach it is assumed that when dislocation loops are large compared to the sphere of influence, i.e. $R_l \geq R_s$, the dislocation loops may be best approximated as straight dislocations of length equal to their circumferences by using the relationship that the corresponding dislocation line density is $2\pi R_lC_l$. In this approximation the growth rates of dislocation loops are given by Eq. (25) corresponding to the case $R_l \geqslant R_s$.

The model based on the system of Eqs. (1)–(17) and Eqs. (18)–(28) was implemented in the MFPR code.

3.1. Applicability range of the dislocation model

In order to determine an applicability range of the dislocation model presented above, results of the test [24] are qualitatively analysed. In this experiment the transient-tested samples came from pellets of the base-irradiated fuel performed under steady-state base irradiation at a maximum linear power of 260 W/cm to an average burn-up of 4.5%, which had been further subjected in a reactor to power increases up to a maximum of 420 W/cm with hold times up to 60 h. The temperature rise after the transient at the fuel periphery was small and the microstructure remained essentially similar to that of the base-irradiated fuel, with similar dislocation densities. The effect of the transient test was to increase the fuel centre temperature by approximately 300 K from a steady-state centerline temperature, causing significant changes to the fuel centre microstructure.

Indeed, in the base-irradiated fuel the average dislocation density was $\approx 2.2 \times 10^{14}\ \mathrm{m}^{-2}$, which was effectively constant with radius (in a qualitative agreement with MFPR calculations presented in Section 5). According to the evaluation of [24], the temperature varied in the radial direction from $0.25T_m \approx 780$ K at the pellet periphery to $0.45T_m \approx 1400$ K in the pellet centre. The dislocations lines were heavily jogged and the structure was typical of climb-induced growth in the high point defect flux. There was no evidence for plastic deformation having occurred during steady state irradiation. As a result of the temperature rise at the fuel centre, the overall dislocation density became significantly lower, with an average value of $6 \times 10^{13}\ \mathrm{m}^{-2}$, and there was evidence that some plastic deformation had occurred.

These observations clearly show that some additional mechanism (unaccounted in the current model) leading to the dislocation density reduction operates at high temperatures (e.g. mutual annihilation of dislocations, release from grains due to sliding under thermal stresses, etc.) Observations of plastic deformations at these temperatures give evidence that the dislocation density reduction mechanism might be associated with dislocation sliding under significant thermal stresses arising in fuel pellets with a high radial temperature gradient.

Naturally, such a dislocation sliding mechanism (with some activation energy at the initial static recovery, which is the energy for dislocation annihilation by glide or cross-slip) does not operate in the peripheral pellet zone where temperature is low and the dislocations are locked and move with difficulty, so that the material will then be brittle. At higher temperatures thermal fluctuations should be sufficient to release the dislocations under the stresses so that the material will be ductile. As demonstrated in [25], the ductile behaviour of (fresh) UO_2 fuel prevails at high temperatures (above $\approx$1200 °C). Therefore, the current dislocation model cannot be applied with confidence to the high-temperature temperature range $\geqslant$1500 K.

4. Model validation

4.1. Experimental data

The new dislocation model implemented in the MFPR code was validated against the experimental data of [1,2]. In these experiments the detailed characteristics of intra-granular bubbles and dislocations in UO_2 fuel pellets in a wide range of burn-ups 6–83 GWd/t under steady irradiation conditions were examined. The maximum irradiation temperatures of the specimens were roughly estimated as 650–750 °C within the accuracy limits ±50 °C.

The measured average bubble diameter increased approximately from a value of 2 nm at a burn-up of ~20 GWd/t to ~6 nm at burn-ups higher than 80 GWd/t. The bubbles concentration increased up to $10^{24}\ \mathrm{m}^{-3}$ at a burn-up of 20 GWd/t, and then slowly decreased within one order of magnitude (approximately $\sim 10^{23}\ \mathrm{m}^{-3}$) at burn-ups greater than 80 GWd/t.

It should be noted that using a constant (default) value for the bubble nucleation factor, F_n = const. (applied, e.g., in [26,27]), the

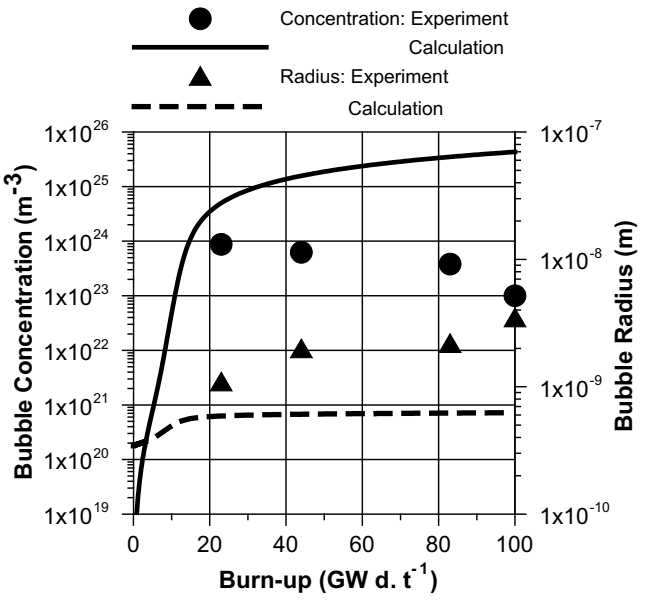

Fig. 1. Calculated intra-granular bubbles concentration and mean bubble radius evolution under steady irradiation conditions as a function of burn-up with the standard constant value of the nucleation factor, $F_n = 10^{-5}$.

MFPR code predicts a strong monotonic growth in the bubble concentration under steady irradiation conditions, Fig. 1, in contradiction with observations of [1,2]. Coupling of the nucleation factor with the vacancy concentration, Eq. (20), allows a more adequate consideration of the irradiation effects on intra-granular bubble evolution in high-burn-up fuel. Indeed, a typical behaviour of the vacancy concentration under steady irradiation conditions calculated by the MFPR code with the implemented defect model is rather non-monotonic as shown in Fig. 2. A strong decrease in the vacancy concentration in late stages of irradiation results in the suppression of the nucleation factor, Eq. (20), and eventually in a pronounced reduction of the bubble concentration, as demonstrated in the following Section 4.2.

4.2. Calculation results

Calculations with the MFPR code were performed for UO_2 fuel with an initial grain diameter 9 nm, porosity 5 % and mean pore radius $R_p = 1$ μm under irradiation at a temperature of 1073 K with the fission rate $F = 10^{19}$ m^{-3} s^{-1} and burn-up of 100 GWd/t. The initial dislocation density and mean vacancy loop radius were chosen as $\rho_0 = 10^{10}$ m^{-2} and $R_{vl} = 1$ nm, respectively.

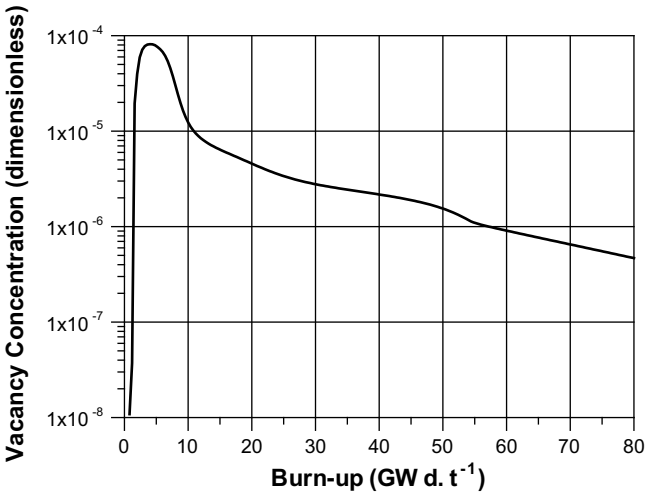

Fig. 2. Calculated vacancy concentration as a function of burn-up under irradiation temperature 1073 K and fission rate 10^{19} m^{-3} s^{-1}.

The re-solution constant b_0 of gas atoms from bubbles was varied in calculations from 2×10^{-23} m^3 to 0.5×10^{-23} m^3 following quantitative evaluation of this parameter in [13]. The parameter of the vacancy cluster formation ξ was varied from 10^{-8} to 10^{-2}; the damage formation in fission tracks factor, z_s, was varied from 1×10^5 to 4×10^5; the vacancy–interstitial recombination radius r_c was varied in the range from 0.5 nm to 5 nm (well corresponding to estimations of [9]). The interstitial bias factor corresponded to the MFPR base set value $2\varepsilon = 3\%$.

The best fit to the experimental data was attained at $\xi \approx 10^{-3}$, $b_0 \approx 0.5 \times 10^{-23}$ m^3, $r_c \approx 1$ nm and $z_s \approx 2 \times 10^5$. The final calculation results with the fixed set of parameters and the new option for the bubble nucleation factor, $F_n = c_v$, are presented in Fig. 3.

Results from validation of the defect model against steady-irradiation experiments show that the main microscopic parameters can essentially differ from the corresponding values typical for metals, despite the basic physical mechanisms of the defect structure evolution being similar in the different materials. Therefore, a similar formalism of the defect model (either for point defects

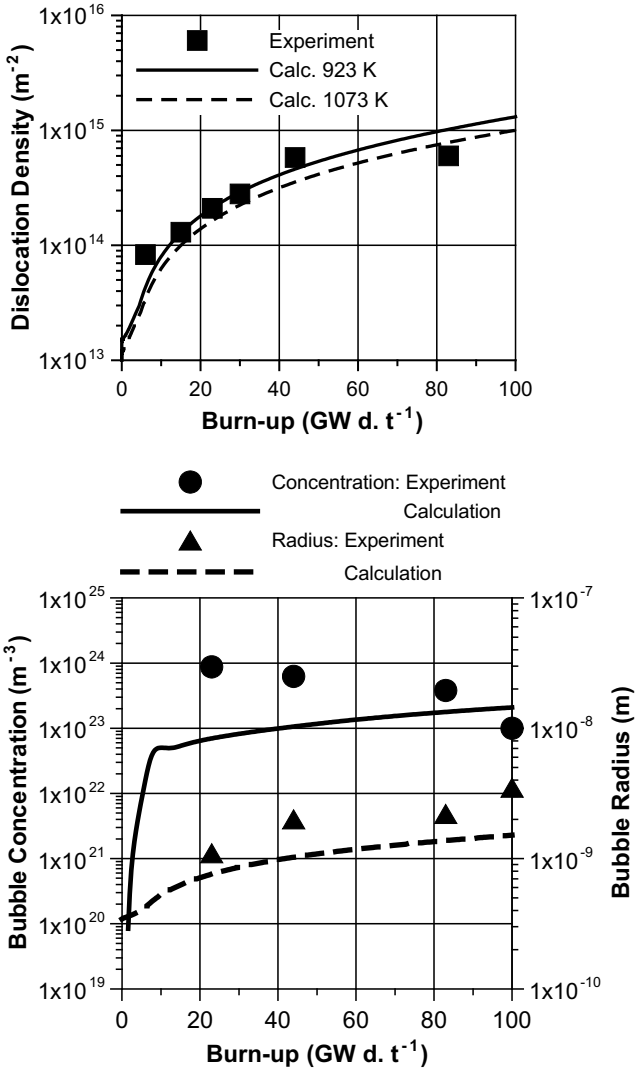

Fig. 3. Calculated dislocations density, intra-granular bubbles concentration and mean bubble radius as a function of burn-up with the new option for the bubble nucleation factor, $F_n = c_v$, in comparison with experimental data [1,2].

[8,10], or for dislocations [21,22]), originally developed for irradiated metals, with a new set of microscopic parameters allows a mechanistic description of the defect system evolution in the ceramic material. In particular, basing on the above–presented calculation results for the dislocation density evolution, the model can be applied (without additional tuning of the microscopic parameters) to high temperatures to provide a mechanistic interpretation of the threshold temperature for the fuel restructuring observed in the rim-zone of high burn-up UO_2 fuel, as demonstrated in the following Section.

5. Model predictions for fuel restructuring at high burn-ups

As observed in [1] at ≈1000 K, tangled dislocation networks with low-angle grain boundaries were formed by the accumulation of dislocations in 44 GWd/t fuel, when the dislocation density attained $\approx 6 \times 10^{14}\ m^{-2}$. For the higher burn-up fuel of 83 GWd/t, dislocations further accumulated and ultimately evolved into sub-divided grains with high-angle boundaries. Similar small subgrains were observed with high resolution transmission microscopy (HRTEM) in UO_2 fuel irradiated with high energy Xe (0.5 MeV), which showed that even in material through which most of Xe-ions have passed without being stopped, subgrain boundaries could form due to the pile up of high density of edge dislocations [28].

The sub-divided grains with high-angle boundaries were postulated in [1] (also in [29]) as the nucleus for the recrystallization of fuel in the rim zone of high burn-up UO_2. This result correlates well with other observations of the burn-up threshold for fuel restructuring between 55 and 82 GWd/t [7].

In accordance with the general theory of cell structure formation [30], dislocation structures tend to develop with increasing dislocation density to form dislocation clusters in which neighbouring dislocations mutually screen their stress field (accepted also in [16]). The cell structure terminates the structural evolution, when the dislocation density attains a certain ultimate value. One can expect that the dependence of this ultimate value on temperature would be rather weak, owing to its physical nature (i.e. stress screening).

From analysis of the above presented test observations [1], the transition from low-angle to large-angle cells occurs in the range of dislocation density from $\approx 6 \times 10^{14}$ to $\approx 10^{15}\ m^{-2}$, Fig. 3, which is correspondingly assumed as the ultimate interval (independent on temperature, as explained above) for further calculations. Application of this ultimate criterion to higher temperatures is presented in Fig. 4 (dashed zone in the dislocation density range from 6×10^{14} to $10^{15}\ m^{-2}$), where the dislocation density evolution with burn-up was calculated by the MFPR dislocation model with microscopic parameters fixed from the analysis of the test [1] in the previous Section 3.2.

At temperatures above 1500 K calculations were not attempted, since this temperature interval is beyond the applicability range of the current dislocation model (see Section 3.1).

From these calculations it is seen that the dislocation density being rather insensitive to temperature at $T \leqslant 1300$ K (in a qualitative agreement with observations of [24] presented in Section 3.1), decreases steeply in the temperature interval from 1300 to 1400 K. The calculated dislocation density drop seems somewhat overestimated (e.g., the dislocation density in the non-restructured central zone of UO_2 pellet with a high burn-up of 74 GWd/t was evaluated with TEM [31] as $\approx 2.5 \times 10^{14}\ m^{-2}$), however, correctly demonstrates the qualitative tendency, and can be smoothed down by further refinement of the model parameters on the base of a more systematic data set for the dependence of dislocation density on temperature (currently unavailable). Example of calculations with

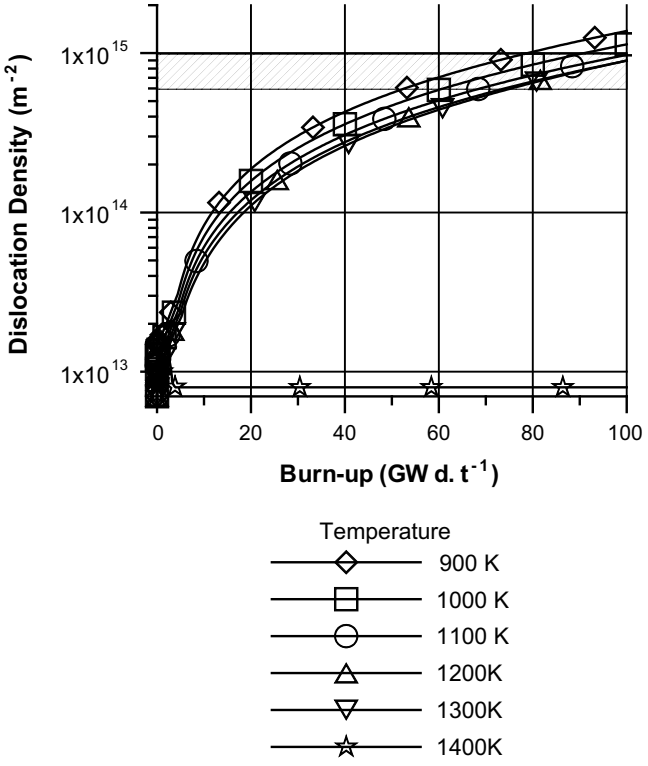

Fig. 4. Dislocations density as a function of burn-up, calculated in steady state irradiation conditions at different temperatures (base set of the model parameters).

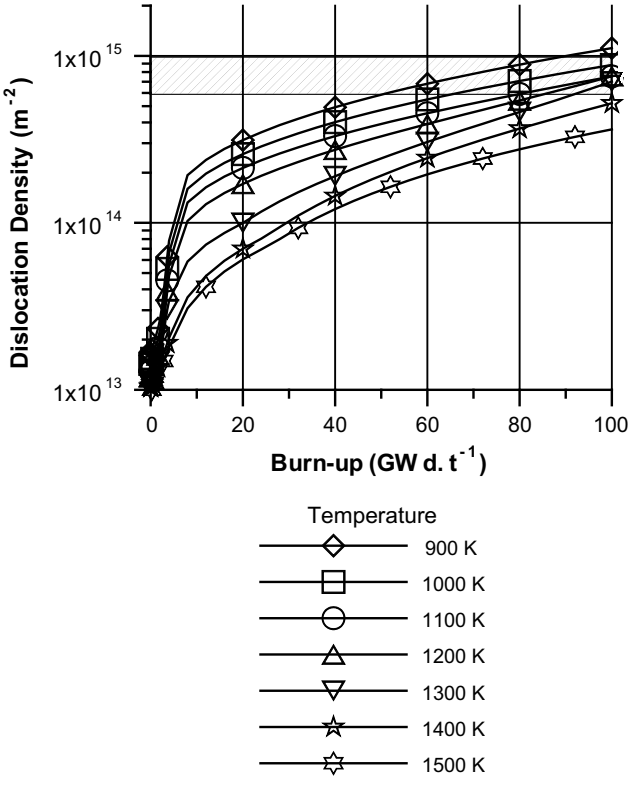

Fig. 5. Dislocations density as a function of burn-up, calculated in steady state irradiation conditions at different temperatures (modified set of the model parameters).

a somewhat modified set of model parameters (also suitable for correct description of the test [1]) is presented in Fig. 5.

Therefore, the calculations show that the ultimate limit for dislocation density is not attained at high temperatures even at very high burn-ups. This model prediction provides a reasonable interpretation of the temperature threshold 1300–1400 K above which no restructuring occurs, at least up to 100 GWd/t, detected in recent observations [7].

Nevertheless, this does not exclude other mechanisms of grain subdivision and fuel restructuring in the rim zone considered in the literature (e.g., interplay with fission gas bubbles and fission product precipitates as well as the effect of soluble fission products in the UO_2 matrix, etc. [32]), which should be considered simultaneously and self-consistently with the dislocation mechanism.

6. Conclusions

The model for dislocations generation and evolution under irradiation conditions was developed and implemented in the MFPR code. Being combined with the MFPR set of microscopic equations for the evolution of point defects and their interactions with gas bubbles, a self-consistent consideration of the whole system of point and extended defects in irradiated fuel, including point defects (vacancies, interstitials and gas atoms), as well as extended defects (bubbles, dislocations, vacancy loops and pores), was attained.

The MFPR code with the new defect evolution model was validated against steady irradiation experiments, in which the dislocation density and the bubble concentration and mean size were directly measured as functions of burn-up. MFPR allows a satisfactory prediction of the considerable suppression of the intra-granular bubble concentration growth accompanied by a noticeable increase of the mean bubble size in the late stage of irradiation, observed in the recent tests with high burn-up UO_2 fuel [2]. Results for the dislocation density evolution obtained in these calculations are also in a reasonable agreement with the high burn-up fuel measurements [1].

Sensitivity study of the new code version against the MFPR basic and new microscopic parameters allows refinement of these parameters. Being physically grounded, these parameters were fixed to attain the best fit to the experimental data [1,2], and then used without any artificial tuning in further calculations. For instance, the MFPR model predicts a noticeable decrease of the dislocation density at high temperatures above 1300–1400 K which can be associated with the temperature threshold for fuel restructuring observed in the rim-zone of high burn-up UO_2 fuel in recent tests [7].

Acknowledgements

This work was supported by IRSN, Cadarache (France) under the Contract on the mechanistic code MFPR development; the personal support and collaboration of Dr. R. Dubourg and Dr. P. Giordano (IRSN) are highly appreciated. The author also thanks Dr. V. Tarasov and Dr. V. Ozrin (IBRAE) for their assistance and collaboration in implementation of the new model in the MFPR code.

This work was also supported by the Russian Foundation for Basic Research which is greatly acknowledged by the authors.

References

[1] K. Nogita, K. Une, Nucl. Instrum. and Meth. Phys. Res. B91 (1994) 301.
[2] S. Kashibe, K. Une, K. Nogita, J. Nucl. Mater. 206 (1993) 22.
[3] M.S. Veshchunov, V.D. Ozrin, V.E. Shestak, V.I. Tarasov, R. Dubourg, G. Nicaise, Nucl. Eng. Des. 236 (2006) 179.
[4] M.S. Veshchunov, R. Dubourg, V.D. Ozrin, V.E. Shestak, V.I. Tarasov, J. Nucl. Mater. 362 (2007) 327.
[5] A.D. Whapham, B.E. Sheldon, Electron Microscope Observation of the Fission-Gas Bubble Distribution in UO_2. AERE-R-4970, 1965.
[6] A.D. Whapham, Nucl. Appl. 2 (1966) 123.
[7] M. Kinoshita, T. Sonoda, S. Kitajima, A. Sasahara, T. Kameyama, T. Matsumura, in: Proceedings of the 2004 International Meeting on LWR Fuel Performance, Orlando, Florida, September 19–22, 2004.
[8] A.D. Brailsford, R. Bullough, Philos. Trans. Royal. Soc. A 302 (1981) 87.
[9] R.J. White, M.O. Tucker, J. Nucl. Mater. 118 (1983) 1.
[10] R. Bullough, B.L. Eyree, K. Krishan, Proc. R. Soc. Lond. A. 346 (1975) 81.
[11] C.C. Dollins, F.A. Nichols, J. Nucl. Mater. 78 (1978) 326.
[12] H. Stehle, H. Assmann, J. Nucl. Mater. 52 (1974) 303.
[13] M.S. Veshchunov, J. Nucl. Mater. 227 (2000) 67.
[14] F. Seitz, Disc. Faraday Soc. 5 (1949) 271.
[15] H.J. Matzke, Adv. Ceram. 17 (1986) 1.
[16] J. Rest, G.L. Hofman, J. Nucl. Mater. 277 (2000) 231.
[17] H.J. Matzke, Radiat. Eff. 53 (1980) 219.
[18] D. Brucklacher, W. Dienst, J. Nucl. Mater. 42 (1972) 285.
[19] R.G.J. Ball, R.W. Grimes, J. Chem. Soc. Faraday Trans. 86 (1990) 1257.
[20] S. Nicoll, H.J. Matzke, C.R.A. Catlow, J. Nucl. Mater. 226 (1995) 51.
[21] M.R. Hayns, J. Nucl. Mater. 56 (1975) 267.
[22] M.H. Yoo, J. Nucl. Mater. 68 (1977) 193.
[23] SCDAP/RELAP5 MOD2 CODE, Manual, vol. 4: MATPRO—A Library of Material Properties for Light Water Reactor Accident Analysis. NUREG/GR-5273, EGG-255, vol. 4, 1990.
[24] I.L.F. Ray, H. Thiele, H.J. Matzke, J. Nucl. Mater. 188 (1992) 90.
[25] A.G. Evans, R.W. Davidge, J. Nucl. Mater. 33 (1969) 249.
[26] T.J. Heames, D.A. Williams, N.E. Bixler, A.J. Grimley, C.J. Wheatley, N.A. Johns, P. Domogala, L.W Dickson, C.A. Alexander, I. Osborn-Lee, S. Zawadzki, J. Rest, A. Mason, R.Y. Lee, VICTORIA: A Mechanistic Model of Radionuclide Behaviour in the Reactor Coolant System under Severe Accident Conditions. NUREG/CR-5545, 1992.
[27] J. Rest, S.A. Zawadzki, FASTGRASS, A Mechanistic Model for the Prediction of Xe, I, Cs, Te, Ba and Sr release from Nuclear Fuel under Normal and Severe-Accident Conditions. NUREG/CR-5840 TI92 040783, 1994.
[28] H.J. Matzke, L.M. Wang, J. Nucl. Mater. 231 (1996) 155.
[29] H.J. Matzke, J. Spino, J. Nucl. Mater. 248 (1997) 170.
[30] N. Hansen, D. Kuhlmann-Wilsdorf, Mater. Sci. Eng. 81 (1986) 141.
[31] I.L.F. Ray, H. Thiele, H.J. Matzke, M. Kinoshita, J. Nucl. Mater. 245 (1997) 115.
[32] M. Kinoshita, T. Kameyama, S. Kitajima, H.J. Matzke, J. Nucl. Mater. 252 (1998) 71.